Silicon nitride C-band grating couplers with reduced waveguide back-reflection

Ibrahim Ghannam*, Florian Merget, Jeremy Witzens
Institute of Integrated Photonics, RWTH Aachen University, 52074 Aachen, Germany

ABSTRACT

In this work, we developed a C-band grating coupler for the 800 nm silicon nitride platform with fully etched grates and reduced back-reflection. To reduce the latter, we present a coupler design in which the first few grates are interrupted in the center of the beam emitted from the waveguide. Their span is gradually increased as the beam propagates deeper into the grating coupler until they cover its entire width. Compared to a conventional reference design, measurements show a reduction of the waveguide-to-waveguide back-reflection in a range of 5 dB to 12 dB over the entire grating coupler passband at the cost of an additional 3 dB insertion losses. These correspond to peak-insertion losses of 8.55 dB and back-reflections below -24 dB across the 40 nm 1-dB bandwidth of the grating coupler, that remains unchanged compared to the reference design. The reduced back-reflection and reference grating couplers have identical pitch and uniform grating period. A method to improve the trade-off between insertion losses and back-reflection strength is also proposed. Simulations indicate that half of the excess losses resulting from the grating coupler modification can be recovered by adapting the shapes of the grates to compensate for incurred phase errors. Elliptical grates with an eccentricity that varies across the grating coupler are chosen as a first order correction.

Keywords: Light coupling, grating coupler, back-reflection reduction, silicon nitride, external cavity lasers

1. INTRODUCTION

Grating couplers (GC) in the silicon-on-insulator (SOI) [1,2] and silicon nitride (SiN) [3,4] platforms permit coupling light from free-space to anywhere on the surface of the chip, which in turn enables flexible routing and denser photonic chips. Research on GCs has focused on achieving low coupling loss [5], wide bandwidth [6], reduced footprint [7], relaxed alignment tolerances [8,9] and reduced back-reflections [10-13]. Waveguide-to-waveguide back-reflections limit in particular the useability of GCs to outcouple light from external cavity lasers (ECLs) [9] or from transceivers with heterogeneously [14] or monolithically integrated lasers [15] that are not provided with an isolator, due to the stability of laser operation being compromised by parasitic feedback. As a consequence, grating-coupler-enabled platforms typically make use of optical isolation in a dedicated laser micro-package [16-18]. Spurious back-reflections can also limit useable power levels in photosensitive materials such as chalcogenides [19].

GC reflections originate mainly from two sources. The first is the second-order Bragg condition, which is mitigated by tilting the fiber and adjusting the grating periodicity. The second is the back-reflection at the boundary between the first grating trenches and the input taper, which is particularly high for fully etched GCs. Multiple ideas of varying complexity have been devised to reduce the second type of back-reflections [10-13]. However, fabrication in a standard foundry process puts many restrictions on the design. In this work, we developed and characterized a GC with fully etched grates that has a reduced back-reflection. This is achieved by changing the span of the first few grates, which leads to changing the field profile of the back-reflected light which is then no longer supported by the input waveguide and scattered out of the GC. This essentially corresponds to an adaptation of idea first reported in [11] to an SiN platform with an 800 nm core film [20], with a different truncation of the grates, slightly better insertion losses and a significant (5 dB) further suppression of overall back-reflection. An approach to further improve the trade-off between insertion losses and back-reflections with adapted grate geometries is also proposed and validated by simulations.

2. GRATING COUPLER DESIGN

Figure 1(a) shows the layout of the nominal GC used to benchmark the back-reflection reducing GCs. The device is a fully etched, focusing GC with a pitch of 1.17 μm and a duty cycle of 44.87%, defined as the ratio of the unetched teeth width to the pitch. Grates are circular, the onset of the first grate is 30 μm from the input waveguide, and the taper spans a full angle of 25.6°. The input waveguide, with a 600 nm width and an 800 nm height, supports a single transverse electric (TE) mode. The device is optimized for peak coupling in the C-band at 1550 nm and outcoupling at a forward angle θ of 11° in SiO$_2$ (fiber array polish angle).

*ighannam@iph.rwth-aachen.de; phone +49 241 80 20020; iph.rwth-aachen.de

The back-reflection reducing GCs are implemented by interrupting the first few grates in the center of the beam incoming from the waveguide and gradually increasing their span. The devices are identical to the nominal one in every other aspect. Figure 1(b) shows a diagram of such a device. The angle φ controls the width of the interrupted grates, wherein the 1st grate fills an angle φ on either side of the GC, the 2nd grate an angle 2φ etc., until the grates fill the full span of the GC.

The PIC was fabricated by LIGENTEC in a high-quality, 800 nm low-pressure chemical vapor deposited (LPCVD) film with fully etched structures clad all-around by SiO_2.
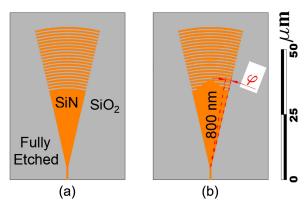

Figure 1. Layouts of (a) nominal focusing grating coupler and (b) modified design with reduced reflections. The angle φ controlling the span of the trenches from the edge of the taper is multiplied by the grate index until grates fill the full taper span. A smaller φ leads to more interrupted grates. The layout in (b) with φ=3.65° corresponds to the device labeled as GC3 in the experiments.

To evaluate the functionality of the GC, a series of 3D finite-difference time-domain (FDTD) simulations were performed. A packet of light, with a peak amplitude at 1550 nm, is launched into the waveguide located on the left of Fig. 2. It shows the intensity of the back-reflected light taken as a snapshot in time when most of the reflected light has reached back to the beginning of the taper, at the waveguide junction. The optical field was recorded on the center plane of the SiN film. For the reference GC, a significant portion of the light packet is reflected back into the TE ground mode of the input waveguide, as shown in Fig. 2(a). In the case of the reduced back-reflection GC with φ = 3.9° simulated in Fig. 2(b), the introduced disruption of the first few grates leads to an oblique reflection and thus to excitation of higher-order modes. These are filtered out as the waveguide supports only the TE ground mode, as visible in Fig. 2(b). This leads to an overall reduction in the power back-reflected into it.
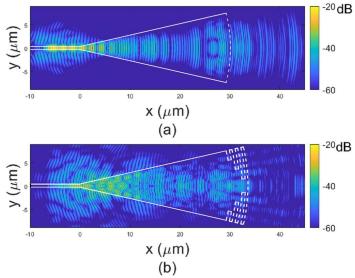

Figure 2. Intensity of the back-reflected light in dB for (a) the nominal GC and (b) the modified GC with 3 interrupted grates (φ = 3.9 degrees). The field intensity was recorded from an FDTD simulation at a time at which most of the back-reflected field reached back to the waveguide junction. The two simulations are identical in their parameters and the same point in time is shown in the two panels.

3. MEASUREMENTS AND BACK-REFLECTION EXTRACTION

Figure 3(a) shows a schematic of the test structure that was used to estimate the back-reflection. Light is sent to one GC and collected from the second, the collected power is measured with a power meter. By sweeping the wavelength of the laser source, the response of the waveguide loop is observed. The laser used in the measurement has a wavelength range from 1510 nm to 1590 nm. The raw data is shown in Fig. 4(a). It can be seen that the transfer function of the waveguide loop is overlaid with ripples characteristic of the waveguide-to-waveguide back-reflections in the system. In addition to the reference GC, two low-reflection GCs have been fabricated, with GC2 and GC3 corresponding to $\varphi = 5.3^\circ$ and $\varphi = 3.65^\circ$, respectively.

To smooth the GC's transfer function, a Sparse Smooth Decomposition (SSD) algorithm is used [21]. The output of the algorithm is the smoothed GC response, an error or noise signal and an anomaly or sparse feature (not present here, that can be extracted in the general case assuming it has a different structure from the main signal, for example if there were periodic ring resonances superimposed). The smoothed responses, divided by two to account for the insertion losses of a single GC, are shown in Fig. 3(b). We can extract the coupling efficiencies and bandwidths from them. The reference GC, GC2 and GC3 have a minimum insertion loss of 5.8 dB, 7 dB and 8.55 dB, respectively, obtained at a wavelength around 1546 nm for all three. The 1-dB bandwidth is 40 nm for all.

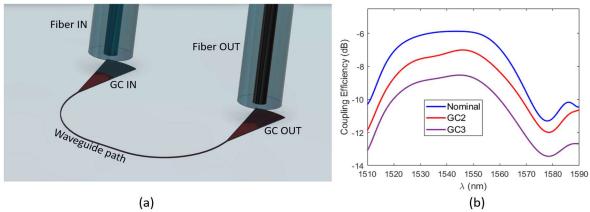| | |
| (a) | (b) |

Figure 3. (a) Schematic of the test structure, the pitch of the GCs is 127 μm, the waveguide length 188 μm. The figure is drawn to scale except for the two fibers. (b) Smoothed coupling efficiencies of the different grating coupler types.

A different procedure based on a Fourier analysis was followed to extract the ripples and the GC back-reflection. The method is an expansion of the procedure used in [19,22]. Figure 4(b) shows the Fourier transform of the transfer functions of the three GCs. Multiple peaks are apparent, however, only the first (indicated by the green box) are relevant here. Indeed, the periodicity of the corresponding ripples corresponds to the free spectral range (FSR) expected from the waveguide loop. The spectra are taken with a 1 pm wavelength resolution over 80,000 points, so that the index of 35 at which the first peak is located corresponds to an FSR of 2.29 nm, very close to the expected 2.3 nm given the group index of the waveguide calculated to be 2.1 and the 248 μm long waveguide loop also taking the lengths of the tapers to the first grates into account. This first peak can be seen to be very clearly attenuated as one goes from the reference design to increasingly modified grating couplers GC2 and GC3. The second peak apparent in the Fourier transforms could be attributed to the measurement setup, as it was present in the recorded spectra irrespective of the length of the measured waveguide loops (we measured devices with waveguide lengths of 188 μm, 484 μm and 1208 μm, and this peak was always there at the exact same position). Consequently, we concluded that this second peak is a measurement artefact and removed it from the analysis. This allowed us to improve the floor of the measurement, i.e., the minimum back-reflection that could be reliably extracted. In order to isolate the relevant peak prior to operating an inverse Fourier transform, the background spectrum corresponding to the smoothed GC transfer function was first subtracted. This background could be well fitted as having an amplitude scaling as the inverse of the index (x-axis of Figs. 4(b) and 4(c)) and a phase scaling linearly with it, facilitating this background removal. A Gaussian band-pass filter is then used to isolate the first peak from the remaining spectrum components, with the result shown in Fig. 4(c). The data is then transformed back with an inverse Fourier transform, resulting in the extracted ripples shown in Fig. 4(d). Finally, the peak-to-peak ripple strength is used to extract the magnitude of the power back-reflection coefficient R according to

$$R = \frac{\sqrt{ER}-1}{\sqrt{ER}+1} \tag{1}$$

where *ER* stands for extinction ratio and describes the magnitude of the ripples, obtained from taking the difference of the peak and minimum transmission on a dB scale in a given cycle and converting it to the linear domain.
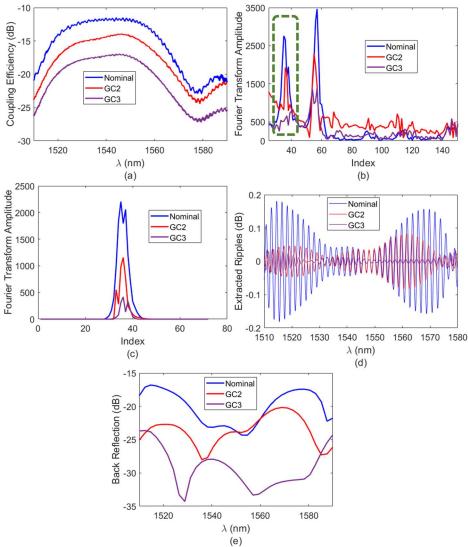

Figure 4. (a) Raw transmission data, (b) Fourier transform of the transmission data in dB, (c) isolated first peak, (d) reversed transformed data showing the extracted ripples, and (e) extracted back-reflection.

Comparing both GC2 and GC3 with the reference design, it appears that GC3 presents the best suppression in back-reflection. A smaller φ, corresponding to a wider interruption in the grates and a larger number of interrupted grates, as well as the formation of steeper facets along the contour of interrupted grates, is thus, as would be intuitively expected, improving the back-reflection suppression. However, as visible in Fig. 3(b), this is also accompanied by an increasing reduction in coupling efficiency. Compared to the reference GC, the coupling efficiency of GC2 is reduced in a range of 1.2 dB to 1.5 dB, while that of GC3 is reduced by about 3 dB. On the other hand, GC2 reduces the back-reflection between -0.7 dB to 5.4 dB, while GC3 reduces it considerably more, between 5 dB and 12 dB. The variations in the measured back-reflection can be caused by a number of factors. For one, the artefacts in the measured data and the data analysis method itself could introduce some deviations. However, it is also possible that interactions between multiple reflections lead to such behavior. For example, in [11] multiple reflections at the tapers' boundaries have been highlighted as a possible cause for ripples observed in the back-reflection spectra.

4. IMPROVEMENT OF THE LOSS-BACK-REFLECTION TRADE-OFF

The observed trade-off between back-reflection suppression and insertion losses is due to some extent to the missing scattered field in the truncated grate region, leading to a further deviation from the targeted Gaussian shaped radiated field profile. However, the distortion of the phase front of the light inside the slab, and consequently of the coupled out field, plays an equally important role. The latter is due to the refractive index perturbation corresponding to truncation of the trenches. It leads to a local perturbation of the field propagating inside the slab and continues to impact the light as it propagates down the grating beyond the region in which the grates have been truncated. Fortunately, this phase error can be compensated by deforming or segmenting the grates and moving them towards the waveguide in the angular sectors in which grates have been left out.
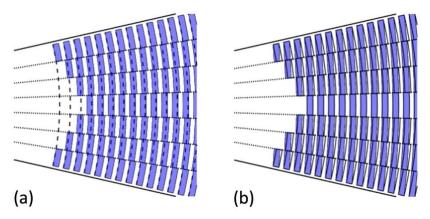

Figure 5. (a) Segmented grates concept. The grating coupler is divided into 7 angular sectors delimited by the dotted lines, with each sector corresponding to a region with a constant number of grates. In the inner sectors, in which grates have been left out, grates are moved towards the waveguide to compensate for the perturbed phase, such that the scattered field is extracted with the correct phase to participate to the targeted flat free-space wavefronts. The dashed curves show the onset of the initial grates, before applying the displacements. (b) Corresponding geometry with smoothed grates. Grates are drawn with an elliptical shape that best follows the position of the segmented grates in (a). The elliptical grates are shown in blue with the outline of the segmented grates overlaid for comparison. The eccentricity is individually adjusted for each grate.

This is conceptually shown in Fig. 5(a) that corresponds to an adaptation of the layout of GC3 ($\varphi = 3.65°$) in which grates have been segmented and displaced by an increment d for every left out grate in a given angular segment given by

$$\frac{2\pi n_{sl}}{\lambda_0} d = \frac{2\pi (n_{sl} - n_{ox})}{\lambda_0} w + \frac{2\pi n_{ox}}{\lambda_0} sin(\theta) d$$

with λ_0 the free-space wavelength, n_{sl} the effective index of the SiN slab (1.88), n_{ox} the refractive index of SiO$_2$ (1.45), w the width of the trenches (645 nm), and θ the angle of the scattered beam in SiO$_2$, as previously described (11°). This results in

$$d = \frac{n_{sl} - n_{ox}}{n_{sl} - n_{ox} sin(\theta)} w$$

which is equal to 173 nm in our case.

In a second step, the segmented grates are approximated by smooth elliptical grates whose eccentricity is chosen such that they best follow the position of the previously determined grate segments, as shown in Fig. 5(b). This is expected to yield better results, since light would be scattered at the discontinuities in the segmented case and would not stay in a given segment. The eccentricity is calculated independently for each grate and varies from 0.85 to 0.64 for the first 20 grates.

The geometry with the elliptical grates shown in Fig. 5(b) is simulated to result in a peak insertion of -7.2 dB, which is only moderately worse (1.6 dB) than the nominal baseline grating coupler (Fig. 1(a)), that is simulated to have -5.6 dB insertion losses. Without elliptical grate adaptation, GC3 is measured to have 8.55 dB insertion losses, which is significantly worse (2.75 dB) than the 5.8 dB measured for the reference design. About half the excess insertion losses resulting from the modification of the reference design into GC3 are thus expected to be recovered by adopting the elliptical grate shape as described above, with further optimization possible. This is not expected to impact the back-reflection reduction in a significant way.

5. CONCLUSION

We have presented a silicon nitride grating coupler design based on truncated grates in which reduced back-reflection is obtained at the cost of increased insertion losses. In the experimentally shown devices, a reduction of back-reflections in the range of 5 dB to 12 dB comes at the cost of a 3 dB reduction in coupling efficiency. To improve this trade-off, we introduce a novel design approach in which the shape of the grates is adjusted to correct for phase errors induced by truncation of the grates. Simulations show that with this approach about half of the 3 dB coupling penalty can be recovered. Experimental demonstration of this design approach is planned.

REFERENCES

[1] Marchetti, R., Lacava, C., Carroll, L., Gradkowski, K., and Minzioni, P., "Coupling strategies for silicon photonics integrated chips," Photon. Res. 7, 201-239 (2019).

[2] Taillaert, D., Van Laere, F., Ayre, M., Bogaerts, W., Van Thourhout, D., Bienstman, P., and Baets, R., "Grating couplers for coupling between optical fibers and nanophotonic waveguides," Jpn. J. Appl. Phys. 45, 6071–6077 (2006).

[3] Romero-García, S., Merget, F., Zhong, F., Finkelstein, H., and Witzens, J., "Silicon nitride CMOS-compatible platforms for integrated photonics applications at visible wavelengths," Opt. Expr. 21(12), 14036-14046 (2013).

[4] Romero-García, S., Merget, F., Zhong, F., Finkelstein, H., and Witzens, J., "Visible wavelength silicon nitride focusing grating coupler with AlCu/TiN reflector," Opt. Lett. 38(14), 2521-2523 (2013).

[5] Marchetti, R., Lacava, C., Khokhar, A., Chen, X., Cristiani, I., Richardson, D. J., Reed, G. T., Petropoulos, P., and Minzioni, P., "High-efficiency grating-couplers: demonstration of a new design strategy," Sci. Rep. 7, 16670 (2017).

[6] Doerr, C. R., Cheng, L., Chen, Y. K., and Buhl, L., "Wide bandwidth silicon nitride grating coupler," IEEE Photon. Technol. Lett. 22(19), 1461 (2010).

[7] Van Laere, F., Claes, T., Schrauwen, J., Scheerlinck, S., Bogaerts, W., Taillaert, D., O'Faolain, L., Van Thourhout, D., and Baets, R., "Compact focusing grating couplers for silicon-on-insulator integrated circuits," IEEE Photon. Technol. Lett. 27, 612–618 (2009).

[8] Romero-García, S., Shen, B., Merget, F., Marzban, B., and Witzens, J., "Alignment Tolerant Couplers for Silicon Photonics," J. Sel. Top. Quant. Electron. 21(6), 8200214 (2015).

[9] Ghannam, I., Ackermann, M., Romero-García, S., Merget, F., and Witzens, J., "Silicon Photonics External Cavity Laser with Alignment Tolerant Multi-mode RSOA to PIC Interface," in Proc. Conf. Las. and Electro-Opt. (CLEO), ATh3I.3 (2019).

[10] Benedikovic, D., Alonso-Ramos, C., Pérez-Galacho, D., Guerber, S., Vakarin, V., Marcaud, G., Le Roux, X., Cassan, E., Marris-Morini, D., Cheben, P., Boeuf, F., Baudot, C., and Vivien, L., "L-shaped fiber-chip grating couplers with high directionality and low reflectivity fabricated with deep-UV lithography," Opt. Lett. 42, 3439-3442 (2017).

[11] Song, J. H., Snyder, B., Lodewijks, K., Jansen, R., and Rottenberg, X., "Grating coupler design for reduced back-reflections," IEEE Photon. Technol. Lett. 30(2), 217–220 (2018).

[12] Zou, J., Zhang, Y., Hu, J., Wang, C., Zhang, M., and Le, Z., "Grating coupler with reduced back reflection using λ/4 offset at its grating sub-teeth," J. Lightwave Technol. 37, 1195–1199 (2019).

[13] Na, N., Frish, H., Hsieh, I.-W., Harel, O., George, R., Barkai, A., and Rong, H., "Efficient broadband silicon-on-insulator grating coupler with low backreflection," Opt. Lett. 36, 2101-2103 (2011).

[14] Tran, M. A., et al., "Extending the spectrum of fully integrated photonics," arXiv:2112.02923 (2021).

[15] Shang, C., Wan, Y., Selvidge, J., Hughes, E., Herrick, R., Mukherjee, K., Duan, J., Grillot, F., Chow, W. W., and Bowers, J. E., "Perspectives on Advances in Quantum Dot Lasers and Integration with Si Photonic Integrated Circuits," ACS Photon. 8(9), 2555-2566 (2021).

[16] Narasimha, A., et al., "An ultra low power CMOS photonics platform for H/S optoelectronic transceivers at less than $1 per Gbps," in Proc. Conf. Opt. Fib. Comm. (OFC), OMV4 (2010).

[17] Snyder, B., Corbett, B., and O'Brien, P., "Hybrid Integration of the Wavelength-Tunable Laser With a Silicon Integrated Circuit," J. Sel. Top. Quant. Electron. 31(24), 3934-3942 (2013).

[18] De Dobbelaere, P., Ayazi, A., Chi, Y., Dahl, A., Denton, S., Gloeckner, S., Hon, K.-Y., Hovey, S., Liang, Y., Mack, M., Masini, G., Mekis, A., Peterson, M., Pinguet, T., Schramm, J., Sharp, M., Sohn, C., Stechschulte, K.,

Sun, P., Vastola, G., Verslegers, L., and Zhou, R., "Packaging of Silicon Photonics Systems," in *Proc. Opt. Fib. Comm. Conf. (OFC)*, W3I.2 (2014).

[19] Shen, B., Lin, H., Sharif Azadeh, S., Nojic, J., Kang, M., Merget, F., Richardson, K. A., Hu, J., and Witzens, J., "Reconfigurable frequency-selective resonance splitting in chalcogenide microring resonators," ACS Photon. 7(2), 499–511 (2020).

[20] Stroganov, A., Geiselmann, M., "Silicon Nitride PICs Platform Development from a Foundry Perspective: From Concepts to Real Applications," in *Proc. Europ. Conf. on Int. Opt. (ECIO)*, (2019).

[21] Yan, H., Paynabar, K., and Shi, J., "Anomaly Detection in Images With Smooth Background via Smooth-Sparse Decomposition," Technometrics 59(1), 102-114 (2017).

[22] Ismail, N., Calil Kores, C., Geskus, D., and Pollnau, M., "Fabry-Pérot resonator: spectral line shapes, generic and related Airy distributions, linewidths, finesses, and performance at low or frequency-dependent reflectivity," Opt. Express 24, 16366-16389 (2016).